Parametric noise squeezing and parametric resonance of microcantilevers in air and liquid environments

Gyan Prakash,[1] Arvind Raman,[2] Jeffrey Rhoads,[2] and Ronald G. Reifenberger[1]
[1]*Birck Nanotechnology Center and Department of Physics, Purdue University, West Lafayette, Indiana 47907, USA*
[2]*Birck Nanotechnology Center and School of Mechanical Engineering, Purdue University, West Lafayette, Indiana 47907, USA*

(Received 19 June 2011; accepted 9 May 2012; published online 20 June 2012)

In this work, parametric noise squeezing and parametric resonance are realized through the use of an electronic feedback circuit to excite a microcantilever with a signal proportional to the product of the microcantilever's displacement and a harmonic signal. The cantilever's displacement is monitored using an optical lever technique. By adjusting the gain of an amplifier in the feedback circuit, regimes of parametric noise squeezing/amplification and the principal and secondary parametric resonances of fundamental and higher order eigenmodes can be easily accessed. The exceptionally symmetric amplitude response of the microcantilever in the narrow frequency bandwidth is traced to a nonlinear parametric excitation term that arises due to the cubic nonlinearity in the output of the position-sensitive photodiode. The feedback circuit, working in both the regimes of parametric resonance and noise squeezing, allows an enhancement of the microcantilever's effective quality-factor (Q-factor) by two orders of magnitude under ambient conditions, extending the mass sensing capabilities of a conventional microcantilever into the sub-picogram regime. Likewise, experiments designed to parametrically oscillate a microcantilever in water using electronic feedback also show an increase in the microcantilever's effective Q-factor by two orders of magnitude, opening the field to high-sensitivity mass sensing in liquid environments. © *2012 American Institute of Physics*. [http://dx.doi.org/10.1063/1.4721282]

I. INTRODUCTION

Parametric resonance and amplification have been exploited in such diverse fields as quantum optics,[1] plasmas,[2] superconducting physics,[3] surface waves in liquid,[4] and electronics.[5] In 1991, Rugar and Grütter[6] extended the use of parametric amplification to microelectromechanical systems (MEMS) when they studied vibrations of an atomic force microscope (AFM) microcantilever pumped electrostatically. Continuing advancement in the design and fabrication of MEMS and nanoelectromechanical systems (NEMS) resonators have made it clear that such resonators can operate at high frequencies[7,8] with high sensitivities[9] and low power requirements,[10] making MEMS/NEMS a promising area for the development of resonant sensors[10–14] and miniaturized precision measurement devices.[15] It is therefore not surprising that parametrically excited MEMS/NEMS devices are receiving increased attention in the literature.[16–23]

The conventional way to excite a mechanical resonator is to apply a periodic external driving force at the natural resonant frequency of the resonator. When the mechanical resonator is an AFM-like Si-microcantilever pinned at one end and operating under ambient conditions, it will typically have a natural resonant frequency in the range of 20–300 kHz with a natural quality-factor (Q-factor) that lies between 100 and 1000, with exact values determined by the detailed geometry of the device and material from which it is made. An alternative to directly driving a microcantilever is to parametrically excite it. Parametric *excitation* is a non-conventional technique that requires a time-periodic variation of the system's impedence, specifically stiffness or mass.[24] When the frequency of parametric excitation is near twice the natural frequency of the resonator, and if the amplitude of the parametric variation is above a threshold value, then *parametric resonance* of the resonator is said to result.[24,25] Secondary parametric resonances are also possible if the resonator is parametrically driven at other frequencies determined by select ratios between the parametric excitation frequency and the natural frequency of the resonator, as well as the exact value of the parametric gain.[24] On the other hand, when the parametric excitation is near twice the natural frequency of an oscillator and the amplitude of the parametric pump is below a threshold value, then *parametric amplification* is said to occur and two different scenarios are possible. If a parametric excitation below threshold gain is applied in combination with direct external excitation near the natural frequency of the system, the steady-state amplitude and phase response of oscillator to external excitation will exhibit an increased effective Q-factor of the resonance line shape due to *parametric amplification*.[26] If a parametric excitation below threshold gain is applied without an external excitation, the resulting amplitude fluctuation at the natural resonance frequency becomes larger than expected from thermal fluctuations alone. In addition, the frequency bandwidth of the thermal fluctuations decreases, an effect often referred to as *noise squeezing*.[6]

Several methods have been implemented to either parametrically excite or parametrically amplify microcantilever

oscillations. Requa and Turner[21] implemented parametric excitation and resonance utilizing the Lorentz force by passing alternating current through a microcantilever placed in a uniform magnetic field. Patil and Dharmadhikari[22] investigated parametric excitation and resonance by periodically moving a substrate to produce a modulation of the van der Waals force acting on a microcantilever. Ouisse *et al.*[27] have theoretically investigated parametric excitation and resonance using the electrostatic force gradient near a biased microcantilever. Lifshitz and Cross[28] exploited the intrinsic residual stress of a microcantilever to implement parametric excitation. Dougherty *et al.*[29] used a time-varying magnetic moment to parametrically excite a microcantilever fitted with a magnetic particle at the free end. Dâna *et al.*[17] achieved parametric excitation by mechanically modifying the second-order nonlinear stiffness of a microcantilever. Other than Ref. 21, the parametric excitation was applied in combination with an external excitation near the natural frequency of the system while keeping the gain below the threshold value. Thus, parametric resonance was not attained; instead parametric amplification was demonstrated.

In this work, we explore the advantages offered by a novel electronic feedback approach in which the deflection of a microcantilever is used in real time to parametrically excite the device. This self-excitation method was first implemented in AFM by Moreno-Moreno *et al.*[30] and a detailed numerical analysis of this electronic feedback technique has appeared previously.[31] An advantage of the electronic feedback approach is that no special microcantilever geometry is required, making the technique easy to implement on a standard AFM. Furthermore, using the same electronic feedback circuit with variable gain, a microcantilever can be readily excited in both the parametric resonance and parametric amplification regimes, for the fundamental and higher-order eigenmodes of the cantilever.

This work reports on a series of experiments performed to identify the relevant nonlinearity that limits the microcantilever oscillation amplitude when operating in the parametric resonance regime and shows that the electronic feedback technique is able to enhance the effective Q-factor of the microcantilever by two orders of magnitude in both the parametric resonance and parametric amplification regimes. Exploiting the parametrically enhanced Q-factor, we show that electronic feedback endows a conventional, off-the-shelf microcantilever with sufficient sensitivity to demonstrate subpicogram mass detection. This can also be achieved by implementing a conventional excitation and tracking phase under vacuum condition or by exploiting the nonlinear jump in the microcantilever response of the microcantilever in air. However, the present implementation of a parametrically excited microcantilever demonstrates a symmetric (Lorentzian or non-Lorentzian) and non-hysteretic microcantilever response, as well as an enhancement of effective Q-factor, and does not require vacuum condition. A further advantage is illustrated by demonstrating a parametric sharpening of the effective Q-factor of a commercially available microcantilever immersed in water, opening the way for fluid-based microcantilever sensing applications with greater sensitivity than previously possible.

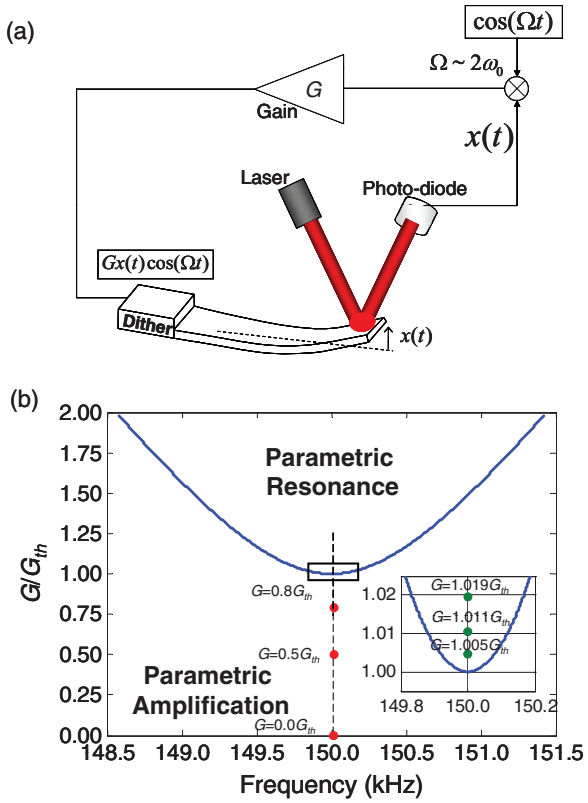

FIG. 1. (a) A schematic of the circuit used to implement the parametric feedback for the microcantilever excitation. (b) The instability tongue for the parametrically excited microcantilever in the parameter space of $G/G_{\rm th}$ vs. Ω. The solid dots are values of G used in the computer simulations. The inset shows an enlarged view of the situation for $G > G_{\rm th}$.

II. THEORY

The parametric excitation of a microcantilever is implemented by feeding back a signal proportional to the microcantilever deflection to the cantilever's piezoelectric mounting stage after multiplying by a time-varying sinusoidal signal of the form of $\cos(\Omega t)$, where Ω is the excitation angular frequency that lies close to twice the natural angular frequency of the microcantilever ($\Omega \sim 2\omega_{\rm o}$). In principle, a voltage signal proportional to the microcantilever deflection can be obtained in many ways, for instance, by measuring the change in capacitance of the microcantilever or changes in the resistance of a thin piezo-resistive thin film bonded to the microcantilever. In this study, we employed a simple optical lever technique where the microcantilever deflection was measured using the voltage output from a quadrant-photodiode as shown in Fig. 1(a).

The theory underlying parametric excitation is well known[24,25] and it is established that the linearized Mathieu's equation describes the linear physics of a parametrically excited microcantilever regardless of the specific method of excitation.[31] The linear Mathieu's equation is given by Eq. (1),[24]

$$\ddot{x} + \frac{\omega_0}{\mathrm{Q}}\dot{x} + \omega_0^2\,(1 - G\cos\Omega t)\,x = 0, \qquad (1)$$

where $x(t)$ represents the deflection of the free end of the microcantilever from its equilibrium position. The

parameter G is an overall gain factor that multiplies the $x(t)\cos(\Omega t)$ feedback signal. The term enclosed by parenthesis in Eq. (1), the equivalent stiffness of the microcantilever, is sinusoidally modulated and it is this effect that parametrically excites the resonator. Q is the quality factor of the eigenmode and represents the ratio of the resonant frequency to the 3 dB width of the resonance response of the system as Ω is varied. The natural frequency of the first eigenmode of the microcantilever is f_0 and the angular resonance frequency $\omega_0 = 2\pi f_0$.

The amplitude of oscillation described by Eq. (1) will continue to grow without bound. To correctly represent a parametrically oscillating microcantilever, the nonlinear behavior of the system must be included by adding a nonlinear term in Eq. (1). As described later, this nonlinearity in the experiments has been determined to be $x^3\cos(\Omega t)$, a nonlinear parametric excitation term. Thus, Eq. (1) must be modified as

$$\ddot{x} + \frac{\omega_0}{Q}\dot{x} + \omega_0^2[1 - G(1 - \delta x^2)\cos(\Omega t)]x = 0, \tag{2}$$

where δ is the coefficient of a cubic nonlinearity in the photodetector. The source of such system nonlinearity is of considerable interest and a detailed analysis of this nonlinearity will be presented in Sec. III below. The theoretical model presented in this work does not include structural nonlinearity as the oscillation amplitude of the microcantilever is maintained very small compared to the microcantilever dimension.

Non-trivial solutions of the linearized Mathieu equation can grow in amplitude and reach a large steady-state value under parametric resonance (i.e., $\Omega \sim 2\omega_0$) provided G is larger than a threshold value, G_{th}.[25] The response of the microcantilever is observed to be non-hysteretic and its width is governed by[30]

$$\left(\frac{\Omega}{\omega_0}\right)^2 = 4 \pm 2\sqrt{G^2 - \frac{4}{Q^2}}, \tag{3}$$

where Ω, ω_0, Q, and G are the parameters as discussed above. From Eq. (3), the threshold value $G_{th} = 2/Q$. Figure 1(b) shows a plot of Eq. (3) where the region inside the parabola represents the unstable region in which parametric resonance can be achieved. Higher-order parametric resonances are also possible. The 2nd and 3rd orders of parametric resonance occur at $\Omega \sim \omega_0$ and $\Omega \sim 2\omega_0/3$, respectively.[25] Outside the instability tongue, the microcantilever demonstrates quasi-periodic oscillations which decay such that only a trivial steady-state solution is obtained.

Before describing the experimental results it is useful to numerically solve Eq. (2) using parameters that closely match experimental conditions. In what follows, two different regimes are investigated, namely, (a) *parametric resonance* and (b) *parametric amplification*. Throughout the theoretical analysis, Q and f_0 were selected to be 300 and 150 kHz, respectively. The microcantilever stiffness was chosen to be 20 N/m.

A. Parametric resonance

Parametric resonance is achieved when the excitation is near twice the natural frequency of the microcantilever ($\Omega \sim 2\omega_0$) and the gain is above the threshold value ($G > G_{th}$).

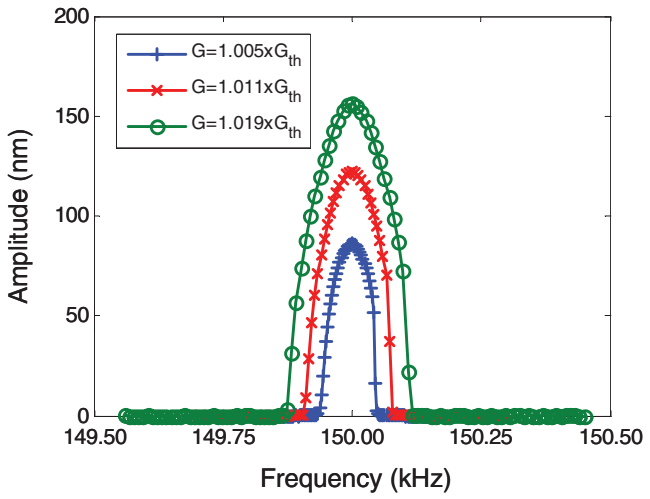

FIG. 2. Numerical simulation of parametric resonance of a microcantilever at different feedback gain (G) values for $G > G_{th}$. These simulations include the nonlinear parametric term, $\delta\, x^3\cos(\Omega t)$, with $\delta = 1 \times 10^{-7}\ \mathrm{m}^{-2}$.

By maintaining the parametric excitation condition $\Omega \sim 2\omega_0$ and selectively adjusting the value of G above threshold, the effective width of the primary resonance peak can be controlled. In the parameter space of Fig. 1(b), parametric resonance is achieved when the system lies within the unstable region bounded by the instability tongue. Simulations for the microcantilever oscillation amplitude using numerical techniques described previously[31] are shown in Fig. 2. As the gain was increased from $1.005G_{th}$ to the $1.019G_{th}$, the resonance peak increased in width as specified by Eq. (3). In these simulations, the coefficient of the cubic parametric nonlinearity was set to be $\delta = 1 \times 10^{-7}\ \mathrm{m}^{-2}$, a value that is consistent with experimental results for our system. Due to the nonlinearity, the steady-state amplitude plotted in Fig. 2 is finite and increases with increasing G. The response of the microcantilever in the parametric resonance regime is found to be non-Lorentzian but remarkably symmetric. The comparison of forward and backward sweep shows that there is no hysteresis in the response of a parametrically resonated microcantilever (figure not shown). This result is in stark contrast with previous parametric excitation studies[21] where Duffing-like nonlinearities make the parametric response bend to the right or left leading to abrupt amplitude jumps and strong hysteresis as the frequency is swept up or down across resonance. The intentional use of the cubic parametric nonlinearity is key to achieving this result; many other nonlinearities lead to sudden amplitude jumps, and an asymmetric and hysteretic amplitude response.[32–34]

B. Parametric amplification

Parametric amplification is achieved when $\Omega \sim 2\omega_0$ and $G < G_{th}$. Under these conditions, the power spectral density (PSD) of thermal fluctuations of the cantilever is squeezed and sharpened near ω_0 above and beyond what is expected from equilibrium thermal fluctuations. To simulate this situation, Eq. (2) must be modified to include a thermal excitation term

as follows:

$$\ddot{x} + \frac{\omega_0}{Q}\dot{x} + \omega_0^2[1 - G(1 - \delta x^2)\cos(\Omega t)]\, x = F_{th}, \qquad (4)$$

where F_{th} represents the thermal drive to the microcantilever when $G < G_{th}$ (parametric amplification regime). F_{th} is the white noise generated by the random number generator in the code. Since the microcantilever does not oscillate through any appreciable amplitude, the photodiode nonlinearity is ignored here. A numerical solution of Eq. (4) provides $x(t)$, the time history of the microcantilever thermal vibration. Under these conditions, the PSD of $x(t)$ provides information about the microcantilever's natural frequency and Q-factor. Unlike parametric resonance, in the parametric amplification regime the microcantilevers continue to demonstrate a Lorentzian response. In this study, the PSD $S_{xx}(f)$ of a discrete data set $x(t)$ is computed by using the *pwelch* subroutine implemented in MATLAB software. Once the PSD of the microcantilever is obtained from $x(t)$, the resonant frequency and Q-factor of the microcantilever can be estimated by fitting the PSD spectra using the analytical formula for $S_{xx}(f)$,

$$S_{xx}(f) = \frac{A}{Q}\frac{f_0}{\left[f_0^2 - f^2\right]^2 + \left(\frac{f \times f_0}{Q}\right)^2}, \qquad (5)$$

where A, Q, and f_o are treated as fitting parameters.

Time series data $x(t)$ were generated using Eq. (4) to simulate parametric amplification. G was increased from $G = 0.0$ (no feedback, the limit of thermal equilibrium) to a value $G = 0.8G_{th}$. Figure 3(a) shows representative plots of the time history of the microcantilever response under parametric amplification for three different values of G. The corresponding PSD for $G = 0.0G_{th}$, $G = 0.5G_{th}$, and $G = 0.8G_{th}$ are shown in Fig. 3(b). By fitting these peaks to Eq. (5), the Q-factor for $G = 0$ was estimated to be 300 (the natural Q-factor of the microcantilever). For $G = 0.5G_{th}$ and $G = 0.8G_{th}$, the effective Q-factor increased and was estimated to be 550 and 6000, respectively. When $0 \le G < G_{th}$, the area under the resonance in the PSD is no longer constrained to be equal to 3/2 k_BT, since energy is being pumped into the microcantilever by an electronic feedback circuit. Accordingly, the microcantilever is no longer in thermal equilibrium with its environment.

In summary, the theoretical considerations discussed above suggest that the electronic feedback circuit should lead to regimes of principal and secondary parametric resonances as well as in the parametric amplification regime. Moreover, the specific form of the cubic parametric term required to saturate the amplitude at a finite value leads to a remarkably symmetric amplitude response in the parametric resonance regime.

III. EXPERIMENTAL CONSIDERATIONS

In what follows, the experimental considerations required to implement parametric excitation using an electronic feedback circuit are discussed. The experimental results for both the parametric resonance and parametric amplification regimes are presented. Also, the initial results for improved microcantilever mass sensing based on both parametric resonance and amplification are presented.

The experiments are performed using a standard, commercially-available Nanotec Electronica (Spain) Cervantes AFM system. No custom modifications are required other than incorporating a parametric feedback circuit. Feedback of the microcantilever's position $x(t)$ to a dither piezo is implemented using the additional electronic feedback circuit shown in the block diagram presented in Fig. 4. Briefly, an excitation signal at frequency Ω is generated by the AFM-controller. After filtering with a high-pass filter, the amplitude is modified by an operational amplifier with an adjustable gain G. This excitation signal is then multiplied by the microcantilever oscillation signal obtained from the voltage output of the position-sensitive photodiode. The resulting signal is passed through a bandpass filter and then fed back to the base of a dither piezo which served as a mount for the microcantilever chip. The signal from the position-sensitive photodiode is monitored by a root-mean-square (rms) chip as shown in Fig. 4. The monitored signal is thus proportional to the rms amplitude of the parametrically resonating microcantilever. In order to record the microcantilever vibration signal, the out-of-plane oscillation signal of the microcantilever is recorded directly from the photodiode. The Nanotec AFM head used in these

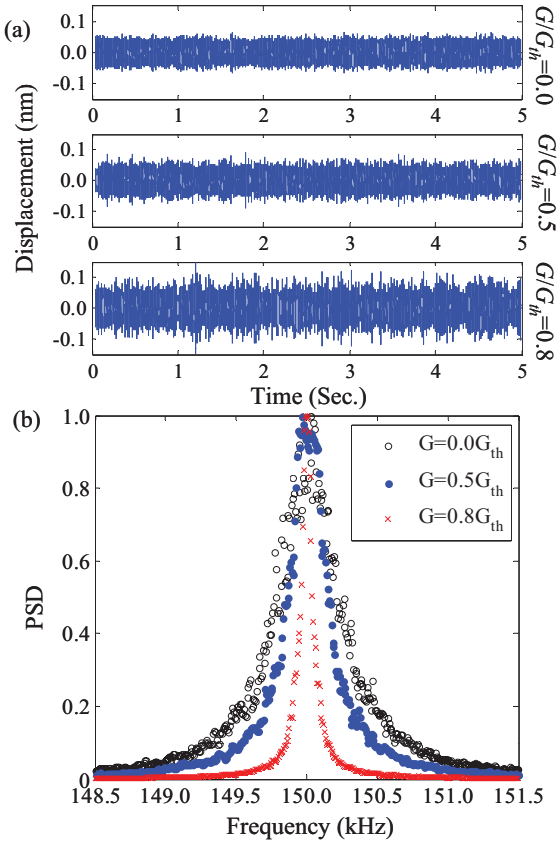

FIG. 3. (a) Numerically simulated time history of the microcantilever fluctuations at different feedback gains, $G = 0.0G_{th}$, $G = 0.5G_{th}$, and $G = 0.8G_{th}$ while excited by white noise. (b) Normalized PSD of thermal vibration of the cantilever "enhanced" by parametric amplification at different feedback gains below G_{th}. The maxima of peaks at $G = 0.5G_{th}$ and $G = 0.8G_{th}$ were 4.5 and 600 times larger than the maximum value of the peak at $G = 0.0G_{th}$, respectively.

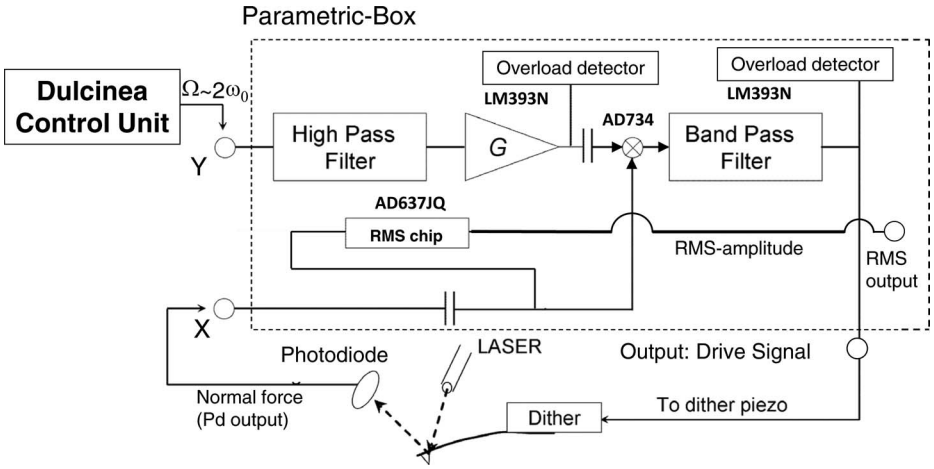

FIG. 4. A schematic diagram of the circuit used to implement parametric excitation. The components are identified using their part number. The various filters were constructed using standard RC networks.

experiments is controlled using WXsM software.[35] The time history of the microcantilever vibration was digitized by a PicoScope Model # 4224 from Pico Technology, United Kingdom. The PSD of the microcantilever's vibration is analyzed by MATLAB using the *pwelch* command.

A systematic analysis is performed to identify the physical source and nature of the $\delta x^3 \cos(\Omega t)$ nonlinearity that appears in Eq. (2) above. The analysis requires the conventional excitation of the microcantilever at the natural frequency of its first eigenmode. The signal from the photodiode is digitized and the signal is analyzed to determine harmonic content. The results of this analysis are summarized in Fig. 5. In Fig. 5(a), the amplitude of the fundamental harmonic is found to increase sub-linearly with drive amplitude. As shown in Fig. 5(b), the amplitude of the 2nd and 3rd harmonics is found to follow a quadratic and cubic dependence with respect to the amplitude of the 1st harmonic signal.

In order to explain these observations, the response of the photodiode $V(t)$ (in volts) is assumed to be $V(t) = y(t) + \gamma y(t)^2 + \delta y(t)^3$, where $y(t)$ is the linear response of the photodiode to the cantilever motion so that $y(t) = V_0 \cos(\omega_0 t)$. We can therefore write

$$\begin{aligned} V(t) &= V_0 \cos(\omega_0 t) + \gamma V_0^2 \cos^2(\omega_0 t) + \delta V_0^3 \cos^3(\omega_0 t) \\ &= \frac{\gamma V_0^2}{2} + \left(V_0 + \frac{3\delta V_0^3}{4} \right) \cos(\omega_0 t) \\ &\quad + \frac{\gamma V_0^2}{2} \cos(2\omega_0 t) + \frac{\delta V_0^3}{4} \cos(3\omega_0 t). \end{aligned} \tag{6}$$

The constant term in Eq. (6) is filtered by the blocking capacitor shown in Fig. 4 and assuming $\delta V_0^3 \ll V_o$, the term multiplying $\cos(\omega_0 t)$ can be further simplified. Since $V_0 \propto x_o$, where x_o is the amplitude of the microcantilever, Eq. (6) indicates the output of the photodiode must have a quadratic and cubic dependence on x_o. Signs of γ and δ are determined by looking at the phase of the response signal of the photodiode at 2nd and 3rd harmonics, respectively. The sign of the coefficients are found to be negative, and are included in Eq. (2). The quadratic nonlinearity has no effect on limiting the amplitude of a parametrically resonating microcantilever

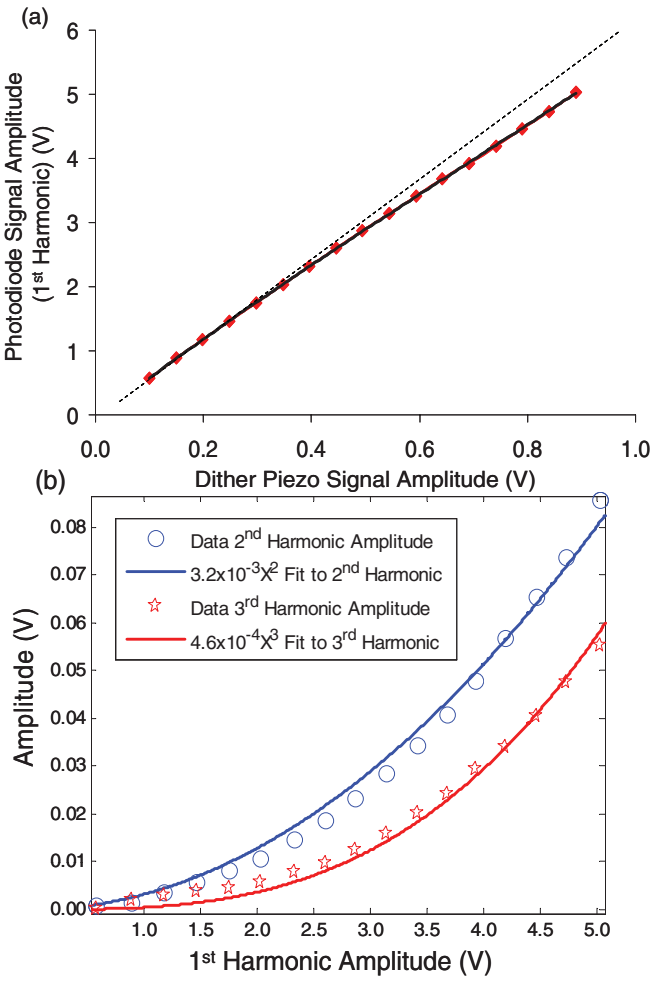

FIG. 5. Identification of the form of dominant nonlinearity in the system. (a) The amplitude of 1st harmonic response signal of a cantilever measured by the photodiode plotted as a function of the excitation amplitude applied to the dither piezo. The amplitude of the 1st harmonic signal is less than the direct proportionality represented by a dotted straight line. (b) Plot of the amplitudes of the 2nd and 3rd harmonic response signal vs. the amplitude of the 1st harmonic signal. Together these results clearly show that the photodiode provides a softening quadratic and cubic nonlinearity which when multiplied with a harmonic signal and fed back to the cantilever lead to a dominant cubic parametric term in the system which dominates the cantilever response in the parametric resonance regime.

because a sinusoidal squared term does not contain a harmonic component at the appropriate harmonic. This was confirmed by using the simulation model described previously.[31] Hence, the relevant nonlinearity present in the system is identified as cubic and parametric in nature, as previously indicated in Eq. (2). Together these results clearly show that the photodiode provides a softening cubic nonlinearity which when multiplied with a harmonic signal and fed back to the cantilever excitation leads to a cubic parametric term in the system which dominates the cantilever response in the parametric resonance regime. This specific form of nonlinearity leads to a well-behaved, nearly symmetric, amplitude response without jumps or significant hysteresis. The system nonlinearity in previous work[30] was assumed to be hydrodynamic in nature. The detail investigation of the system revealed that the primary source of nonlinearity is the photodiode, which leads to a cubic parametric term in the system.

Once the nature and source of nonlinearity is established, it is worth exploring how such nonlinearity leads to Eq. (2). To understand why this circuit leads to a parametric resonance of the cantilever, consider a simple single degree of freedom model of the cantilever dynamics. Let m be the modal mass of the cantilever and tip, k be the modal stiffness or cantilever spring constant, and c be the velocity proportional modal damping coefficient representing linear hydrodynamic losses. Let $z(t)$ be the base motion of the dither piezo, $x(t)$ the instantaneous displacement of the tip, both quantities being measured in an inertial reference frame. The photodiode detects the bending of the cantilever $x(t)-z(t)$ which is amplified by a gain G before feeding back to the dither piezo. Therefore, the dither piezo motion must obey an equation of the form

$$z(t) = G[x(t) - z(t) - \gamma\{x(t) - z(t)\}^2 - \delta\{x(t) - z(t)\}^3] \times \cos(\Omega t), \tag{7}$$

where G is the overall gain of the optical measurement system and γ, δ represent the nonlinearities described earlier. Note that an arbitrary dc component is removed by the high pass filter of the feedback circuit.

Near resonance, $x(t) \cong Qz(t)$, where in air, the quality factor Q is typically greater than 100. Thus, $z(t) \ll x(t)$ and we can write Eq. (7) as

$$z(t) = G \cdot D(t)[x(t) - z(t)]\cos(\Omega t) \tag{8}$$

with $D(t) \equiv 1 - \gamma x(t) - \delta x(t)^2 + z(t)\{\gamma + 2\delta x(t) - \delta z(t)\}$,

$$\equiv 1 - \gamma x(t) - \delta x(t)^2 + O\left(\frac{1}{Q}\right).$$

This finally gives

$$z(t) = G[1 - \gamma x(t) - \delta x(t)^2][x(t) - z(t)]\cos(\Omega t). \tag{9}$$

Rearranging the terms in Eq. (9), we get

$$z(t) = G[1 - \gamma x(t) - \delta x(t)^2]\cos(\Omega t) \times [1 + G\{1 - \gamma x(t) - \delta x(t)^2\}\cos(\Omega t)]^{-1}.$$

Assuming G $\ll$ 1, taking a Taylor expansion of the terms in the rectangular parenthesis and ignoring the higher order terms we get

$$z(t) = G[1 - \gamma x(t) - \delta x(t)^2]\cos(\Omega t). \tag{10}$$

Thus, the equation of motion for the point mass model of the microcantilever with electronic feedback is given by

$$m\ddot{x}(t) + c\dot{x}(t) + k[1 - G\{1 - \gamma x(t) - \delta x(t)^2\} \times \cos(\Omega t)]x(t) = 0. \tag{11}$$

By substituting $c/m = \omega_0/\mathrm{Q}$ and $k/m = \omega_0^2$ and ignoring the quadratic term (discussed earlier) in Eq. (11), Eq. (2) is obtained. The force imparted to the base can be estimated from the base motion as $F_{\text{base}} = md^2z(t)/dt^2$. We note that if $D(t)$ is constant, the feedback will cause the cantilever oscillation to grow without bound.

IV. EXPERIMENTAL RESULTS

A. Characterization of microcantilever response in the parametric resonance and parametric noise squeezing regimes

In order to experimentally study the microcantilever response in the parametric resonance and parametric amplification regions using an electronic feedback technique, a standard, commercially-available microcantilever (Applied Nanostructures, model ACLA-ss) with a nominal frequency of 190 kHz and a stiffness of 45 N/m was used. The natural Q-factor of the microcantilever was measured to be 350 $\pm$ 6 as determined from standard AFM measurements of the conventional frequency response as shown in Fig. 6. Also plotted in Fig. 6(a) is the parametric resonance response with $G = 1.03G_{\text{th}}$. Under parametric resonance conditions, the effective Q-factor of the microcantilever is easily increased from 350 to 3000.

The different orders of parametric resonance of a microcantilever as predicted by theory[25] have been realized in the fundamental and second eigenmode as shown in Fig. 6. Figure 6(a) shows the primary parametric resonance experimentally obtained in the primary eigenmode of the microcantilever. In Fig. 6(b), the primary, secondary, and tertiary parametric resonances are shown for the first and second eigenmode. Each peak shows a sharp parametric curve. The insets show an enlarged representative parametric peak from each eigenmode. The height of the peaks depends on the feedback gain of the parametric resonance. In this study, these gains were arbitrarily selected above the threshold value for each eigenmode.

Separate experiments on a different cantilever were conducted to demonstrate that sharp secondary and tertiary parametric resonance peaks are also observed at specific values of the excitation frequency but at a gain higher than the threshold value of the primary parametric resonance. The secondary parametric resonance is observed when the excitation frequency Ω is equal to that of the natural frequency of the microcantilever (f_o) whereas, tertiary parametric resonance is obtained when the excitation frequency is 2/3 f_o. The secondary and tertiary parametric resonance peaks for the first eigenmode of a microcantilever with f_o = 166.45 kHz are plotted in Fig. 6(b).

A similar study was conducted for the second eigenmode of the same microcantilever with an expected resonant frequency $f_2 \cong 6.3f_o$. The secondary parametric resonance is

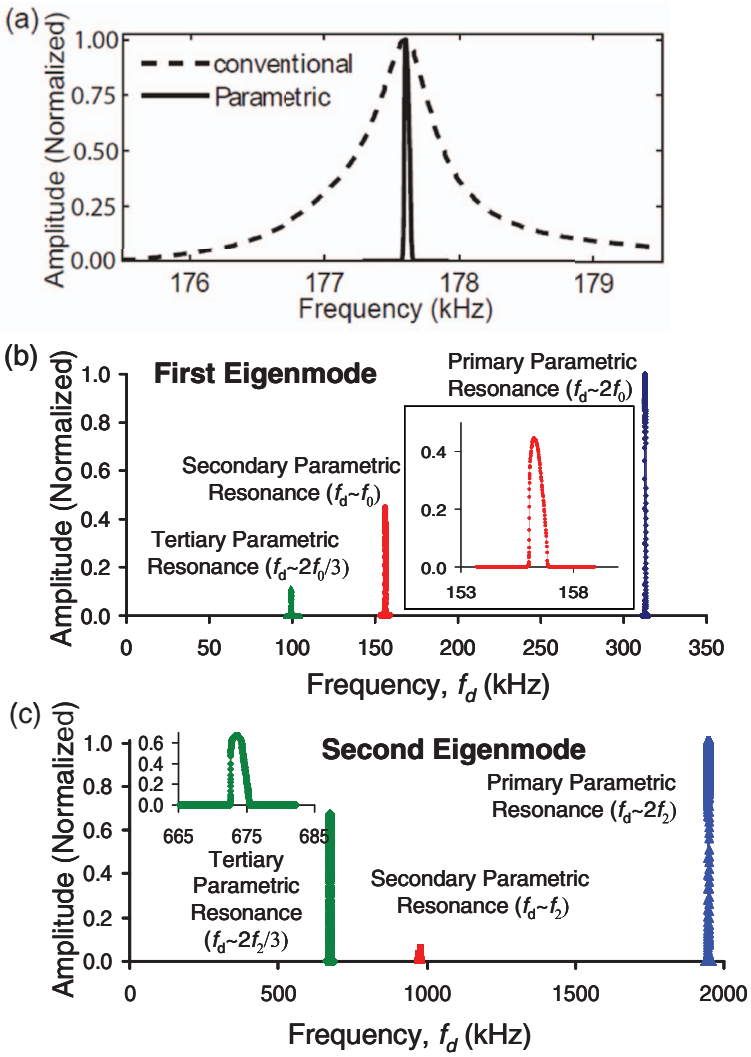

FIG. 6. In (a), the parametric resonance response of a microcantilever in air is compared to the conventional resonance peak obtained by driving the cantilever base using a dither piezo. In this experiment, the parametric gain is set to $G = 1.03^{*}G_{\text{th}}$. The effective Q-factor of the microcantilever is modified from a value of 350 to 3000. In (b), the Primary Parametric Resonance (PPR, blue), Secondary Parametric resonance (SPR, red) and Tertiary Parametric Resonance (TPR, green) peaks of a microcantilever excited in the first eigenmode are shown when the excitation frequency (f_d) is set to be $2f_0$, f_0 and $2f_0/3$, respectively. The gain for each peaks are different and set above the threshold values. The inset shows a zoomed in SPR peak. The natural frequency f_0 of the first eigenmode is 156.45 kHz. In (c), the PPR (blue), SPR (red) and TPR (green) peaks of a microcantilever excited in the second eigenmode are shown when the excitation frequency (f_d) is set to be $2f_2$, f_2 and $2f_2/3$, respectively. The inset shows a zoomed in TPR peak. The natural frequency f_2 of the second eigenmode of the microcantilever is 974.4 kHz. The gain for each peak is different and in each case was set above the threshold value

observed when the excitation frequency is equal to that of the natural frequency of the second eigenmode of the microcantilever (f_2) whereas tertiary parametric resonance is obtained when the excitation frequency is 2/3 f_2. Sharp secondary and tertiary parametric resonance peaks for the second eigenmode of the microcantilever with f_2 measured to be 974.4 kHz were observed as the gain was increased above threshold, as shown in Fig. 6(c).

The parametric amplification regime was also investigated by using the same electronic feedback technique while maintaining G below the G_{th} value. Under these conditions, a measurable sharpening of resonance peak was observed through analysis of the time series displacement data. Plots of the PSD are provided for the response of the first eigenmode of the microcantilever under parametric amplification for $G = 0$ (Fig. 7(a)); $G = 0.6$ (Fig. 7(b)); and $G = 0.9$ (Fig. 7(c)). A systematic study of the effective Q-factor of the resonance peak in air is plotted in Fig. 7(d) and indicates that as G approaches G_{th}, the effective Q-factor of the parametrically amplified microcantilever in air increases from its nominal value of 350 to ~12 000.

The behavior of a parametrically amplified microcantilever was also investigated under water. It is known that under liquids, the microcantilever undergoes fluidic damping and the effective mass of the microcantilever increases. Consequently, the Q-factor is greatly reduced and the resonance frequency decreases significantly.[36] For a similar microcantilever driven conventionally under water, the resonance frequency and Q-factor were measured to be 75.8 kHz and 6, respectively. As G was gradually increased, the resonance peak of the microcantilever sharpened significantly, as shown in Figs. 8(a)–8(c). The systematic increase in the effective Q-factor as G approaches G_{th} is shown in Fig. 8(d). By implementing parametric amplification in a fluidic environment

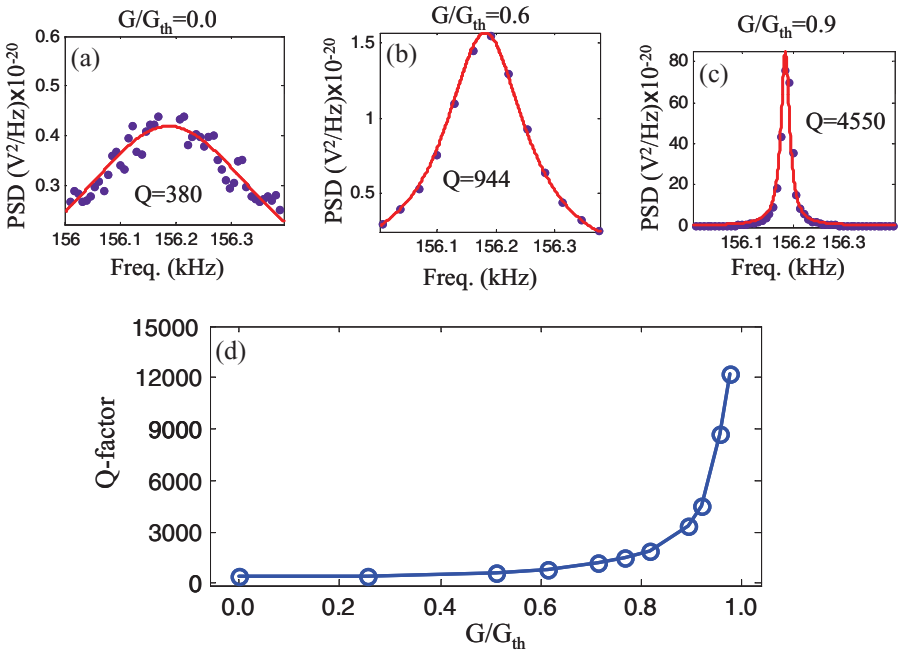

FIG. 7. (a) Power spectral density (PSD) plot of microcantilever intrinsic vibration without any parametric feedback ($G = 0$) in air. In (b) and (c), the PSD of the microcantilever's intrinsic vibrations at gain ratios (G/G_{th}) of 0.6 and 0.9, respectively. (d) Plot of effective Q-factor vs. gain ratio in the regime of parametric amplification. The solid line is a guide to the eye.

under water, the effective Q-factor of the microcantilever was increased from an initial value of 6 to 1500.

In this work, large feedback gains ($G > 1.2G_{th}$) are avoided to keep vibration amplitudes $\ll 1$ μm. The feedback gain in this work is maintained close to the threshold value, in order to achieve small amplitude (~50 nm) and a sharp resonance peak.

B. Mass sensing in air

As discussed above, it has been established that the effective Q-factor of a microcantilever can be increased in both the parametric resonance and the parametric amplification regimes using a simple electronic feedback circuit. This offers obvious advantages for mass sensing and the detection

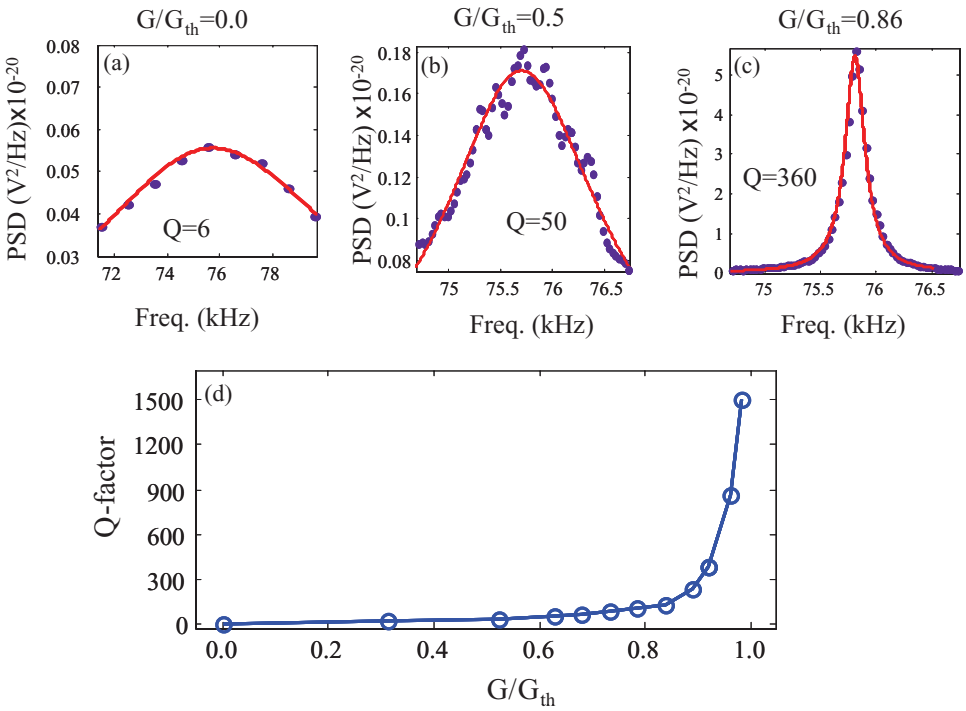

FIG. 8. (a) Power spectral density (PSD) plot of microcantilever intrinsic vibration without any parametric feedback ($G = 0$) in water. In (b) and (c), the PSD of the microcantilever's intrinsic vibrations at gain ratios (G/G_{th}) of 0.5 and 0.86, respectively. (d) Plot of effective Q-factor vs. gain ratio in the regime of parametric amplification. The solid line is a guide to the eye.

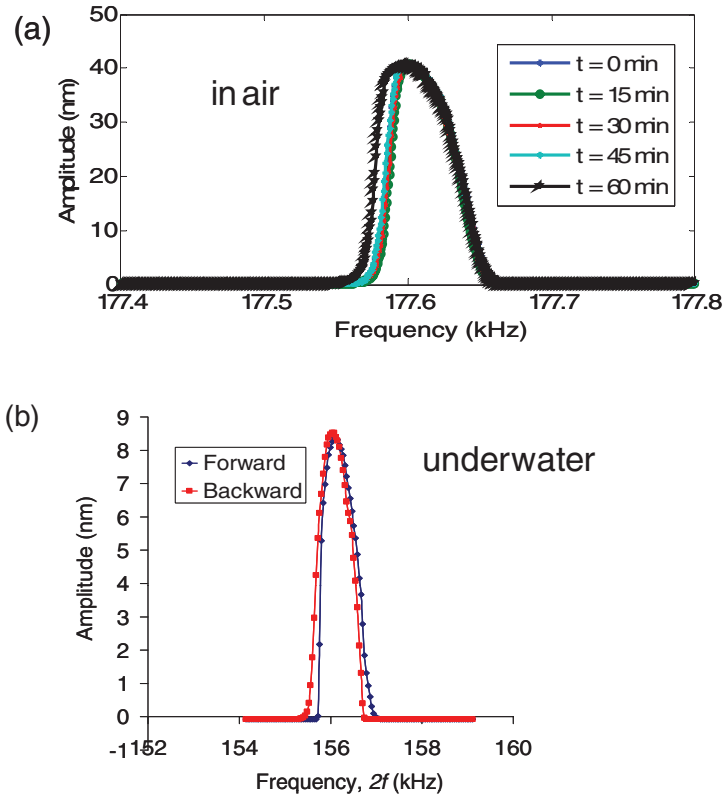

FIG. 9. The stability of the parametric electronic feedback system is demonstrated. In (a), a time dependent study of the resonance when the microcantilever is resonated in air. The abscissa represents half of the excitation frequency. The parametrically resonant microcantilever shows a drift of 3 Hz in 1 h. This drift is equivalent to the error of 6% in the mass sensitivity. In (b), a second experiment in which a cantilever is driven parametrically under water. The abscissa represents half of the excitation frequency. The data are for forward and backward sweeps and demonstrate the non-hysteretic behavior of the resonance.

of analytes and particles in various environments. In what follows, mass sensing in both regimes is demonstrated.

1. Mass sensing in the parametric resonance regime

A concern that arises with narrow resonance peaks is whether the system is sufficiently stable to exploit the beneficial properties of the sharpened resonance. This question was investigated by studying the stability of the resonance response of a parametrically excited microcantilever as a function of time under ambient conditions. This experiment was conducted after allowing the AFM electronics to warm up for ~2 h. The laser spot was optimized on the microcantilever and the resonance peak of the microcantilever was recorded to observe the stability of the resonance peak. As shown in Fig. 9(a), under ambient conditions the shape of the resonance curve of the parametrically resonant microcantilever undergoes a drift of 3 Hz in 1 h. This drift is equivalent to the 6% of the mass sensitivity. Further experiments were conducted to determine if the resonance peak exhibited hysteretic behavior, with a shape that depends on whether the drive frequency is increasing or decreasing with time. No hysteretic behavior was observed. Figure 9(b) plots representative data acquired during forward and backward frequency sweeps while the cantilever is under water.

The stability of the system can be utilized to demonstrate a parametrically driven mass sensor. In order to non-intrusively change the mass of a microcantilever, a micrometer-size particle of the hygroscopic compound $CaCl_2$ was glued to the free end of the microcantilever as shown in Fig. 10(a). $CaCl_2$ is known to absorb moisture from the ambient environment and thus change its mass. Initially, the microcantilever was placed in a dry nitrogen environment and the resonance peak of the parametrically driven microcantilever was recorded. By exchanging dry nitrogen with ambient air, the mass of the hygroscopic $CaCl_2$ attached to the tip could be controllably and reproducibly changed. In these experiments, a microcantilever (Vendor Nanosensors: Model PPP-NCLR) with nominal frequency of 190 kHz and a stiffness of 48 N/m was used. The parametric feedback gain was set at $G = 1.01G_{th}$. Initially, the Q-factor of the microcantilever was 550 whereas under parametric resonance, the Q-factor of the microcantilever increased to 16 000.

While slowly introducing ambient air into the AFM chamber, the frequency response of this $CaCl_2$-microcantilever was recorded using both conventional excitation and parametric excitation every 2 min. One set of frequency response curves is shown in Fig. 10(b). The inset shows a magnified view of the peak-shift observed for parametric resonance. The downshift in the resonance frequency, measured from the shift in the parametric resonance peak, was found to be 11 Hz. It was not possible to measure this shift in resonance frequency from the conventional amplitude resonance peak. The phase shift of the microcantilever oscillation has the ability to demonstrate similar sensitivity in air;

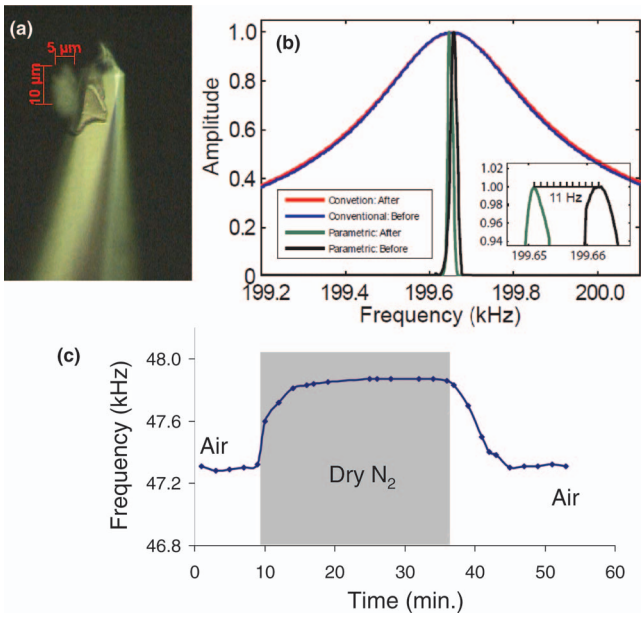

FIG. 10. In (a), an optical image of a hygroscopic particle of $CaCl_2$ attached to the apex of a microcantilever. In (b), a comparison of the resonance peaks from a parametrically and conventionally resonating microcantilever, as humidity is increased by introducing air in the chamber originally filled with dry nitrogen. As air is introduced into the AFM chamber, a downshift in the parametric resonance peak is observed whereas there is no visible shift in the conventional resonance peak. For conventional excitation, the abscissa represents the excitation frequency whereas for parametric excitation, the abscissa represents half of the excitation frequency. The inset shows the measured frequency shift in more detail. In (c), the results of a second time-dependent study which illustrates the frequency shift of a microcantilever with an attached hygroscopic particle of $CaCl_2$ (natural frequency 47.3 kHz) as the chamber is cycled between dry N_2 and air.

however, it deteriorates significantly in fluidic environment. The change in mass of the hygroscopic $CaCl_2$ is reversible as shown in Fig. 10(c). Using a different microcantilever with natural frequency of first eigenmode 47.3 kHz, the frequency shift was reversible as the chamber was filled with dry N_2 and again when backfilled with air.

The mass sensitivity for a microcantilever-based mass-sensor when a mass Δm is added near the free end of the cantilever is given by

$$\Delta m/m = -2\Delta f/f_0, \tag{12}$$

where m is the modal mass of the microcantilever, f_o represents the natural frequency of the first eigenmode, and Δf represents the change in the frequency of the first eigenmode. We conservatively estimate that the smallest shift in resonant frequency that can be directly measured using the parametrically resonant microcantilever is of the order of 1 Hz, allowing an estimate for the mass sensitivity of $\Delta m/m \sim 1 \times 10^{-5}$. For this microcantilever (dimensions: $225 \times 38 \times 7\ \mu m^3$, material: silicon), the modal mass (35×10^{-9} g) is defined as 0.24 of the cantilever mass, suggesting that the minimal detectable mass change of this parametrically driven microcantilever is about 350×10^{-15} g under ambient air conditions.

2. Mass sensing in the parametric amplification regime

It is well known that polydimethylsiloxane (PDMS) can non-selectively absorb volatile organic molecules.[37,38] We exploit this capability to perform further mass sensing experiments using PDMS to change the mass of the microcantilever. In these experiments, the free end of the microcantilever is first coated with PDMS. The microcantilever with affixed PDMS is mounted on an AFM head enclosed by a glass bell jar chamber and backfilled with dry nitrogen gas.

In order to monitor the frequency response of the parametrically driven microcantilever, a time series of vibration response is recorded for approximately 20 s. During data acquisition, Ω is slowly swept through $2\omega_0$. After 20 s, a PSD is then calculated to identify the resonant frequency of the microcantilever. This data acquisition procedure is required because the microcantilever does not oscillate in the parametric amplification regime. Thus, the resonant frequency can only be extracted from a calculation of the PSD.

A microcantilever (Nanosensors model: PPP-NCLR) with a nominal resonant frequency of 190 kHz (in air) and a stiffness of 45 N/m was used. The natural frequency of the microcantilever after adding PDMS dropped to 155.4 kHz. The excitation frequency Ω is varied over the interval 304 kHz $< \Omega <$ 316 kHz in a 20 s interval. The gain of the electronic feedback circuit is set to $G = 0.3G_{th}$ (parametric amplification).

The time history of the PDMS-coated microcantilever, while sweeping Ω, is first recorded in dry nitrogen. Toluene in a petri dish is then introduced into the chamber and left for 60 min before again recording the time history of the microcantilever's position while sweeping Ω. A plot of the PSD for these two cases is plotted in Fig. 11 and shows a clear shift in the resonance peaks. The estimated frequency shift is observed to be 38.5 Hz. Using Eq. (12), the mass-sensitivity is estimated as $\Delta m/m = -2\Delta f/f_0 = 5 \times 10^{-4}$.

C. Parametric amplification in liquids

It is useful to investigate parametric excitation of a microcantilever under a liquid since heavy fluid damping severely compromises microcantilever performance.[36] For instance, under water, the resonance frequency of an intermittent-mode microcantilever drops from a typical value of 190 kHz in air down to 73.45 kHz, while the Q-factor of 550 in air drops to a Q-factor of 6 in water. The low Q-factor significantly deteriorates the mass-sensing ability of the microcantilever. Moreover, under acoustic excitation of a microcantilever in liquid, multiple modes of the cantilever are excited.[39,40] Often, the measured frequency response shows a "forest" of peaks[41–43] due to the resonances of the liquid cell or that of the dither piezo, making it difficult if not impossible to identify the resonant frequency of a desired eigenmode. Due to a low Q-factor and the presence of multiple peaks, the mass-sensing capabilities of a microcantilever immersed in a liquid are significantly reduced.

Exciting a microcantilever in water using parametric resonance solves many of the problems mentioned above. In

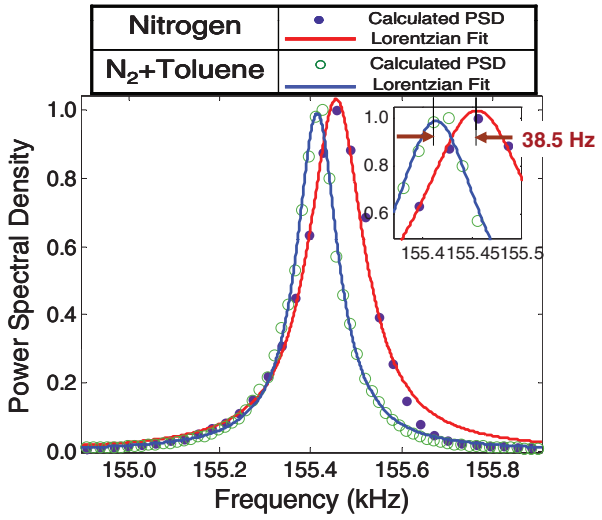

FIG. 11. The normalized PSD of a PDMS coated microcantilever before and after exposure to toluene vapor. The red data points highlight the measured response of a parametrically amplified microcantilever operating under nitrogen. The natural Q-factor of the microcantilever is 400. With G set to $0.3G_{th}$, the effective Q-factor increases to 1000. The blue data points highlight the measured response of a parametrically amplified microcantilever after exposure to toluene vapor. The solid lines are best fit to the data.

Figure 12, the submerged response of a conventionally driven (base-excitation) microcantilever is compared with a parametrically resonant microcantilever using the electronic feedback technique. With the gain set at $G = 1.01G_{th}$, the effective Q-factor was significantly enhanced to a value of 1500, an improvement by two orders of magnitude over that found when the microcantilever's base is excited with a piezo-drive. More importantly, the parametric response does not show any signature of multiple peaks simply because these resonances require a greater gain before they can be parametrically excited. Thus, we find that a parametrically resonant microcantilever in fluid is a key technique required to implement a sensitive microcantilever-based mass sensor in liquid. Figure 12 further

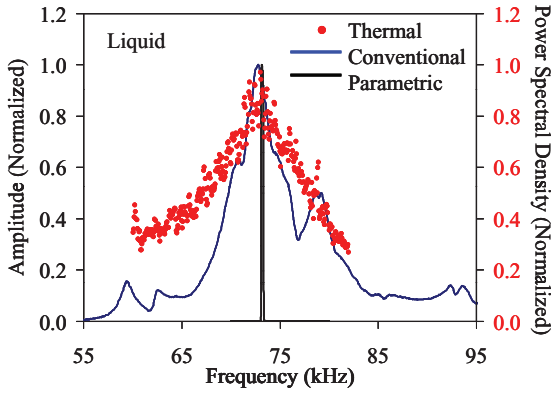

FIG. 12. Comparison of the resonance peaks of the parametrically (in black) and the conventionally (in blue) resonating microcantilever in water. The microcantilever is oscillated piezoelectrically at the base. For conventional excitation, the abscissa represents the excitation frequency whereas for parametric excitation abscissa represents half of the excitation frequency. Both the excitation peaks are also compared with the thermal spectrum shown in red solid circles. The conventional excitation shows multiple peaks whereas parametrically excited microcantilever shows a sharp resonance peak.

demonstrates the advantages offered by parametric amplification to enhance the Q-factor of the vibrating microcantilever in water, making it also a promising candidate for developing a mass sensor in water. One of the potential applications for such a mass sensor in water is to detect the presence of biological samples in fluidic environment, which is the goal of ongoing research.

V. CONCLUSIONS

This work studied an electronic feedback circuit that can be used to implement parametric resonance and noise squeezing in microcantilevers. The intentional design of a nonlinear parametric excitation component in the circuit enables very symmetric amplitude response in the parametric resonance regime with no amplitude jumps and little hysteresis, leading to remarkably sharp, well-behaved amplitude peaks that are ideal for mass sensing applications. The experiments have shown that the effective Q-factor of commercially available AFM microcantilevers can be increased by two orders of magnitude using either excitation regime under ambient air and liquid environments. Implementing this scheme under liquids led to an elimination of the "forest" of peaks and a remarkably sharp resonant response, which opens the path to liquid based mass sensing applications. The use of parametrically resonant and noise squeezed microcantilevers for sensing the uptake of water vapor and absorption of toluene vapors was demonstrated. We anticipate that the electronic feedback circuit implementation of parametric resonance will not only lead to great improvements in mass sensing of cantilevers in both ambient and liquid settings but will also open the door to the easy implementation of narrow band pre-amplifiers and narrow band filters used in high frequency electronic circuits.

ACKNOWLEDGMENTS

A.R. thanks the National Science Foundation (NSF) for partial financial support of this research under Grant No. CMMI- 0700289. We would like to thank Luis Colchero of Nanotec Electronica for the design and construction of the parametric circuit used throughout this study.

[1]L. Wu, H. J. Kimble, J. L. Hall, and H. Wu, Phys. Rev. Lett. **57**, 2520 (1986).
[2]R. Movshovich, B. Yurke, P. G. Kaminsky, A. D. Smith, A. H. Silver, R. W. Simon, and M. V. Schneider, Phys. Rev. Lett. **65**, 1419 (1990).
[3]E. Esarey, P. Sprangle, J. Krall, and A. Ting, IEEE Trans. Plasma Sci. **24**, 252 (1996).
[4]K. Kumar, A. Bandyopadhyay, and G. C. Mondal, Europhys. Lett. **65**, 330 (2004).
[5]R. Ludwig and P. Bretchko, *RF Circuit Design: Theory and Applications* (Prentice-Hall, Upper Saddle River, New Jersey, 2000).
[6]D. Rugar and P. Grütter, Phys. Rev. Lett. **67**, 699 (1991).
[7]M. L. Roukes, Phys. World **14**, 25 (2001).
[8]X. M. H. Huang, C. A. Zorman, M. Mehregany, and M. L. Roukes, Nature (London) **421**, 496 (2003).
[9]K. L. Ekinci and M. L. Roukes, Rev. Sci. Instrum. **76**, 061101 (2005).
[10]X. L. Feng, C. J. White, A. Hajimiri, and M. L. Roukes, Nat. Nanotechnol. **3**, 342 (2008).
[11]Y. T. Yang, C. Callegari, X. L. Feng, K. L. Ekinci, and M. L. Roukes, Nano Lett. **6**, 583 (2006).
[12]J. M. Nichol, E. R. Hemesath, L. J. Lauhon, and R. Budakian, Appl. Phys. Lett. **95**, 123116 (2009).

[13]I. Mahboob and H. Yamaguchi, Appl. Phys. Lett. **92**, 173109 (2008).
[14]J. F. Rhoads, S. W. Shaw, K. L. Turner, J. Moehlis, B. E. DeMartini, and W. Zhang, J. Sound Vib. **296**, 797 (2006).
[15]M. D. LaHaye, O. Buu, B. Camarota, and K. C. Schwab, Science **304**, 74 (2004).
[16]K. L. Turner, S. A. Miller, P. G. Hartwell, N. C. MacDonald, S. H. Strogatz, and S. G. Adams, Nature (London) **396**, 149 (1998).
[17]A. Dâna, F. Ho, and Y. Yamamoto, Appl. Phys. Lett. **72**, 1152 (1998).
[18]J.-P. Raskin, A. R. Brown, B. T. Khuri-Yakub, and G. M. Rebeiz, J. Microelectromech. Syst. **9**, 528 (2000).
[19]M. Zalalutdinov, A. Olkhovets, A. Zehnder, B. Ilic, D. Czaplewski, H. G. Craighead, and J. M. Parpia, Appl. Phys. Lett. **78**, 3142 (2001).
[20]T. Ono, H. Wakamatsu, and M. Esashi, J. Micromech. Microeng. **15**, 2282 (2005).
[21]M. V. Requa and K. L. Turner, Appl. Phys. Lett. **88**, 263508 (2006).
[22]S. Patil and C. V. Dharmadhikari, Appl. Surf. Sc. **217**, 7 (2003).
[23]B. J. Gallacher, J. S. Burdess, and K. M. Harish, J. Micromech. Microeng. **16**, 320 (2006).
[24]A. H. Nayfeh and D. T. Mook, *Nonlinear Oscillations* (Wiley, New York, 1979).
[25]R. Rand, in http://audiophile.tam.cornell.edu/randdocs/nlvibe52.pdf (Internet-first University Press, 2003).
[26]D. W. Carr, S. Evoy, L. Sekaric, H. G. Craighead, and J. M. Parpia, Appl. Phys. Lett. **77**, 1545 (2000).
[27]T. Ouisse, M. Stark, F. Rodrigues-Martins, B. Bercu, S. Huant, and J. Chevrier, Phys. Rev. B **71**, 205404 (2005).
[28]R. Lifshitz and M. C. Cross, Phys. Rev. B **67**, 134302 (2003).
[29]W. M. Dougherty, K. J. Bruland, J. L. Garbini, and J. A. Sidles, Meas. Sci. Technol. **7**, 1733 (1996).
[30]M. Moreno-Moreno, A. Raman, J. Gomez-Herrero, and R. Reifenberger, Appl. Phys. Lett. **88**, 193108 (2006).
[31]G. Prakash, S. Hu, A. Raman, and R. Reifenberger, Phys. Rev. B **79**, 094304 (2009).
[32]Z. H. Feng, X. J. Lan, and X. D. Zhu, Int. J. Non-Linear Mech. **42**, 1170 (2007).
[33]S. Rutzel, S. I. Lee, and A. Raman, Proc. R. Soc. London, Ser. A **459**, 1925 (2003).
[34]M. Yaman, J. Sound Vib. **324**, 892 (2009).
[35]I. Horcas, R. Fernández, J. M. Gómez-Rodríguez, J. Colchero, J. Gómez-Herrero, and A. M. Baro, Rev. Sci. Instrum. **78**, 013705 (2007).
[36]X. Xu and A. Raman, J. Appl. Phys. **102**, 034303 (2007).
[37]M. W. Toepke and D. J. Beebe, Lab Chip **6**, 1484 (2006).
[38]J. N. Lee, C. Park, and G. M. Whitesides, Anal. Chem. **75**, 6544 (2003).
[39]A. Maali, C. Hurth, T. Cohen-Bouhacina, G. Couturier, and J. P. Aime, Appl. Phys. Lett. **88**, 163504 (2006).
[40]M. K. Ghatkesar, T. Braun, V. Barwich, J.-P. Ramseyer, C. Gerber, M. Hegner, and H. P. Lang, Appl. Phys. Lett. **92**, 043106 (2008).
[41]C. A. J. Putman, V. Igarashi, and R. Kaneko, Appl. Phys. Lett. **66**, 3221 (1995).
[42]W. Han, S. M. Lindsay, and T. Jing, Appl. Phys. Lett. **69**, 4111 (1996).
[43]C. Carrasco, P. Ares, P. J. de Pablo, and J. Gómez-Herrero, Rev. Sci. Instrum. **79**, 126106 (2008).